Research Square

Preprints are preliminary reports that have not undergone peer review.
They should not be considered conclusive, used to inform clinical practice,
or referenced by the media as validated information.

Matched Static Feedback Permits Different Notch-Delta Patterning Dynamics

Hyeonje Yang

yangh j0206@snu.ac.kr

Seoul National University https://orcid.org/0009-0007-5151-0528

Research Article

Keywords: Notch-Delta, Feedback Gain, Development, Neuron

Posted Date: November 4th, 2026

DOI: https://doi.org/10.21203/rs.3.rs-11191766/v2

License: This work is licensed under a Creative Commons Attribution 4.0 International License.
Read Full License

Additional Declarations: The authors declare no competing interests.

Matched static feedback permits different Notch–Delta patterning dynamics

Hyeonje Yang
Department of Biological Sciences, Seoul National University
Seoul, Republic of Korea
yanghj0206@snu.ac.kr

Abstract

Notch–Delta lateral inhibition amplifies differences between neighbouring cells, but its steady-state response leaves several dynamical predictions unresolved. We compare explicit signalling circuits while successively matching their static response, mean downstream response time and local linear spectrum. Static loop gain fixes stationary onset. For a negative graph mode, sufficiently strong cis inactivation makes the mode block sign-similar to a Metzler matrix; static gain then gives a necessary and sufficient stability criterion. This condition holds at 775 of 4,000 reference parameter sets; all 12 disagreements between the static-gain test and the full K-mode spectrum lie outside this regime. At a reference patterning point, replacing finite ASC relaxation by its matched quasi-static response raises the K-mode growth rate from 0.103 to 1.597. Dividing the downstream response into four stages at the same mean time makes a uniform oscillation grow faster than the stationary K pattern. Finally, circuits with identical local linear spectra can select different ASC-high cells within the same competent patch. These comparisons connect graph-based gain criteria to explicit pathway kinetics and identify which predictions require information beyond the static response.

1 Introduction

Notch–Delta lateral inhibition provides a contact-dependent mechanism by which initially similar cells acquire distinct signalling states. Delta activates Notch in a neighbouring cell, and the downstream Notch response suppresses proneural activity and Delta production. Classical models established that this feedback can destabilise a homogeneous state [1]. Receptor–ligand cis interactions and contact geometry further constrain the resulting patterns [2–4]. In Drosophila, Notch-dependent Enhancer-of-split expression and the restriction of proneural Achaete–Scute complex activity motivate an explicit downstream layer [5–7].

The presence of this layer raises a comparison that a stationary threshold cannot settle. If two models have the same complete steady-state response, which predictions still depend on downstream kinetics? A finite response time may change the rate at which contrast grows. Its distribution across several stages may also change the competition between stationary and oscillatory modes. Even matching the linear response leaves open whether nonlinear selection depends on where those stages act.

The analysis below addresses these comparisons in a four-variable circuit. Spatial-mode analysis of juxtacrine and networked lateral-inhibition systems is established [8, 9]; it is combined here with standard feedback tools [10]. The comparisons hold static responses fixed while changing response time, pathway resolution or molecular realisation. We identify a cis/trans condition that makes static gain an exact stability test for a negative mode, then isolate the kinetic information needed to predict growth, mode competition and molecular selection.

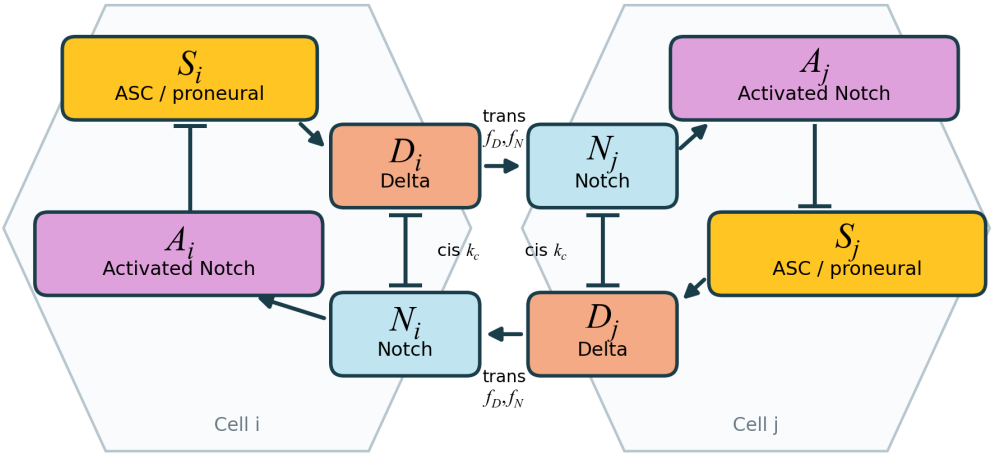


Figure 1: The Notch–Delta–ASC feedback circuit. Two contacting cells are shown in the layout of the supplied schematic. ASC promotes Delta; neighbour Delta activates Notch signalling, and activated Notch represses ASC. Blunt terminals indicate repression or mutual cis inactivation (k_c). Trans interactions include ligand and receptor depletion (f_D, f_N); their arrows indicate signalling, not production of receptor N.

2 Model and matched comparisons

2.1 An explicit contact-coupled circuit

Each cell i carries Delta ligand D_i, Notch receptor N_i, activated-Notch or NICD-like activity A_i, and aggregate proneural Achaete–Scute complex activity S_i. All activities, time and parameter values are dimensionless. Cells contact through a symmetric adjacency matrix W, with no self-contact. The neighbouring activity is the sum $u_{X,i} = \sum_j W_{ij} X_j$, without degree normalisation. The reference graph is a periodic 24×24 triangular contact lattice, with six contacts per cell.

Delta activation and proneural repression are described by

$$h_D(S) = \frac{S^{n_D}}{K_d^{n_D} + S^{n_D}}, \qquad h_S(A) = \frac{K_d^{n_S}}{K_d^{n_S} + A^{n_S}}. \tag{1}$$

Fixed competence $\chi_i > 0$ scales proneural production. Define the static proneural response $q_i(A) = \chi_i \lambda_S h_S(A)/d_S$. The full circuit, with finite ASC relaxation, is denoted AS in the figures and source data:

$$\begin{aligned} \dot{D}_i &= \lambda_D h_D(S_i) - d_D D_i - f_D D_i u_{N,i} - k_c N_i D_i, \\ \dot{N}_i &= \lambda_N - d_N N_i - f_N N_i u_{D,i} - k_c N_i D_i, \\ \dot{A}_i &= f_N N_i u_{D,i} - d_A A_i, \\ \dot{S}_i &= d_S[q_i(A_i) - S_i]. \end{aligned} \tag{2}$$

The production rates are $\lambda_D, \lambda_N, \lambda_S$; the first-order loss rates are d_D, d_N, d_A, d_S. The coefficients f_D, f_N describe the two trans-interaction terms, and k_c describes cis inactivation. The two Hill exponents are n_D, n_S, and K_d is their common half-response activity. Their reference values are given in Table 1. Homogeneous calculations use $\chi_i = 1$. Operating points P2 and P3 change only λ_N to 2 and 5.623, respectively.

2.2 Spatial modes and feedback gain

A graph mode satisfies $W v_\mu = \mu v_\mu$. The uniform mode has $\mu = 6$; the minimum graph eigenvalue, $\mu = -3$, corresponds to three interpenetrating sublattices and is called the K mode. Linearisation

Table 1: Reference parameters. All values are dimensionless. Sampling bounds are specified in Methods.

Parameters	Values	Meaning
$\lambda_D, \lambda_N, \lambda_S$	$5, 1, 1$	Production rates
d_D, d_N	$0.1, 0.1$	Delta and Notch loss
d_A, d_S	$1, 0.1$	Activated-Notch and proneural loss
f_D, f_N	$0.05, 0.6$	Trans-interaction coefficients
k_c	0.35	Cis-inactivation coefficient
K_d	0.3	Hill half-response activity
n_D, n_S	$3, 3$	Hill exponents

at the homogeneous equilibrium gives a four-state Jacobian J_μ for each mode. A pole is an eigenvalue of this Jacobian, and its real part gives the exponential growth or decay rate.

The stable three-state D, N, A plant is denoted B_μ. At equilibrium, let $\mathbf{b} = (\lambda_D h'_D(S^*), 0, 0)^T$ and $\mathbf{c}^T = (0, 0, \lambda_S h'_S(A^*))$, where a star denotes an equilibrium value. With complex frequency s, the instantaneous-downstream loop is

$$L_{0,\mu}(s) = \frac{\mathbf{c}^T (sI - B_\mu)^{-1} \mathbf{b}}{d_S}, \qquad L_\mu(s) = L_{0,\mu}(s) H(s), \qquad G(\mu) = L_{0,\mu}(0). \tag{3}$$

AS has $H(s) = (1 + s/d_S)^{-1}$. Setting $S_i = q_i(A_i)$ instead gives the matched three-state quasi-static ASC reduction (QSS), with $H = 1$. The full nonlinear static response, every equilibrium and the stationary boundary are identical in these two models. Under the positive-feedback convention of Eq. 3, the closed-loop characteristic factor is $1 - L_\mu(s)$; Nyquist encirclements are therefore counted around $+1$.

2.3 Response time, pathway resolution and molecular location

Compensated turnover, $(\lambda_S, d_S) \mapsto \alpha_S(\lambda_S, d_S)$, changes the ASC response time $\tau_S = 1/d_S$ while preserving q_i. To distinguish mean response time from response shape, one relaxation is also replaced by r equal stages:

$$H_r(s) = \left(1 + \frac{s\bar{\tau}}{r}\right)^{-r}. \tag{4}$$

Here $\bar{\tau}$ is the fixed mean downstream response time; the response-time variance is $\bar{\tau}^2/r$. A nonlinear realisation filters $q_i(A_i)$ through r serial linear relaxations of rate $r/\bar{\tau}$, with the last state supplying S_i. It preserves the entire static response for every r.

A separate control changes the location of memory. An effective E(spl)-like mediator obeys $\tau_E \dot{E}_i = A_i - E_i$. The filtered-repressor model (AE) sets $S_i = q_i(E_i)$ immediately, whereas the two-stage repressor–ASC model (AES) retains $\tau_S \dot{S}_i = q_i(E_i) - S_i$. Their downstream filters are

$$H_{\mathrm{AE}} = \frac{1}{1 + s\tau_E}, \qquad H_{\mathrm{AES}} = \frac{1}{(1 + s\tau_E)(1 + s\tau_S)}. \tag{5}$$

E is an effective repressor control, not a calibrated gene product. Equal τ_E and τ_S match AS and AE linear responses; exchanging these times within AES also preserves the complete linear loop. These comparisons test molecular placement separately from pathway resolution at a fixed mean.

3 Results

3.1 Static gain fixes stationary onset but does not fix dynamics

The homogeneous equilibrium is positive and unique for every positive parameter set. A scalar-bracketed solver recovers equilibria at all 4,000 reference points, of which 1,453 (36.325%) have a

nonuniform instability. The equilibrium construction and the feedback identities are given in Supplementary Section S1.

The largest static gain occurs at the most negative graph eigenvalue for every positive parameter set. Thus the first stationary instability selects the K eigenspace on this lattice. Along the reference λ_N continuation, the pole crossing and $G(-3) = 1$ occur independently at $\lambda_N^c = 1.304815343$. At P2, 21 distinct nonuniform graph eigenvalues are unstable.

Gain below unity is insufficient to establish stability. Twelve reference points have $G(-3) < 1$ but two unstable poles in the same K-mode block: six complex pairs and six real pairs. Sample 1730 has $G(-3) = 0.365644$ and poles approximately $0.159 \pm 0.262i$. Adding an E response with $\tau_E = 10$ stabilises every graph mode while retaining the same static gain (Fig. 2B). The K-mode Nyquist count changes from two to zero. This failure of the static test occurs within the tested mode; it is not explained by another mode becoming dominant.

Graph-based criteria connect the static cell response to the spectrum of the contact network [9]. In the present circuit, write $J_\mu = J_{\mathrm{loc}} + \mu UV$, where U maps neighbour inputs to state derivatives and V selects the emitted Delta and Notch activities. The static input–output matrix $\mathcal{T}_0 = -VJ_{\mathrm{loc}}^{-1}U$ gives

$$\det J_\mu = \det J_{\mathrm{loc}} \det(I - \mu\mathcal{T}_0).$$

This graph input–output representation and the ASC-loop gain give the same stationary boundary. Arcak's framework assumes stable fixed-input cell equilibria and monotone cell input–output dynamics. Under these assumptions, its instability criterion is $\lambda_{\min}(P)\rho(T'(u^*)) < -1$, where P is the normalised contact operator, T is the static cell input–output characteristic and ρ denotes spectral radius. His normalised contact operator is $W/6$ here, with K eigenvalue $-1/2$. Mode-block positivity alone does not establish Arcak's cell-level assumptions.

Cis/trans balance identifies a regime in which the static test is exact. For a negative graph mode, consider

$$k_c \geq -\mu \max(f_D, f_N), \qquad \mu < 0. \tag{6}$$

Under this condition, $QJ_\mu Q$ is Metzler (all off-diagonal entries are nonnegative) for $Q = \mathrm{diag}(1, -1, -1, 1)$, and J_μ is Hurwitz if and only if $G(\mu) < 1$ (Supplementary Section S1). At K, the condition is $k_c \geq 3\max(f_D, f_N)$. It holds in 775 reference samples, of which 256 are unstable, with no gain-test disagreements. All 12 disagreements lie among the remaining 3,225 samples, including 1,197 unstable cases. Cis/trans balance therefore determines a regime where the static test is exact; outside this regime, stability can require the frequency-dependent response. The reference point lies outside this regime ($k_c = 0.35 < 3f_N = 1.8$), yet its K block is stable and $G(-3) = 0.455836 < 1$; violating the condition does not force a gain-test disagreement.

Matching the stationary boundary does not match growth. At P2, AS predicts a K-mode rate of 0.103067, compared with 1.597479 for QSS. Compensated turnover varies the AS rate while leaving the static response and threshold unchanged (Fig. 2A). Exact-eigenvector starts recover the predicted early growth within prespecified small-amplitude windows (Fig. S1A). QSS grows faster at every AS-unstable point in the reference design, with a median ratio of 4.90. Ten independent 4,000-point designs give a pooled median ratio of 5.41. These are properties of the specified parameter designs, not biological prevalence estimates.

3.2 Response shape changes the leading instability at a fixed mean

Consider a stable downstream filter with a nonnegative impulse response of unit area. Its transfer function satisfies $H(0) = 1$ and $|H(i\omega)| \leq 1$. Two quantities then bound what changing the pathway can accomplish. If $G(\mu) > 1$, a positive real closed-loop root persists for every such filter. If the peak gain $M_\mu = \sup_\omega |L_{0,\mu}(i\omega)|$ is strictly below one, no such filter can destabilise that mode. The remaining region is unresolved by these sufficient certificates and requires the

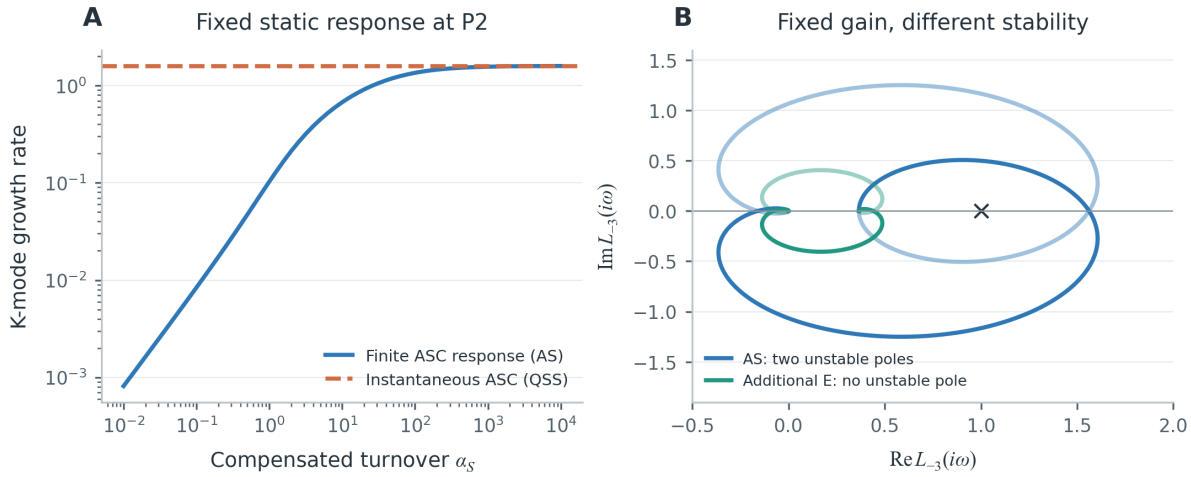


Figure 2: Equal static feedback permits different dynamics. (A) Compensated ASC turnover at P2 changes the K-mode growth rate while preserving the static response and stationary threshold. The dashed line is the matched quasi-static ASC reduction (QSS). (B) K-mode Nyquist curves for reference sample 1730, before and after adding E relaxation with response time 10. Both have DC gain 0.365644; the numbers of unstable poles are two and zero, respectively. The cross marks +1, and lighter lines show conjugate branches. All times and rates use dimensionless model units.

actual pathway response. It does not guarantee instability for an arbitrarily prescribed mean response time.

The Erlang comparison in Eq. 4 holds both static response and mean time fixed. At P2 with $\bar{\tau} = 10$, increasing the depth from $r = 1$ to $r = 4$ reduces the stationary K-mode rate from 0.103067 to 0.075479. Meanwhile, the uniform mode acquires a growing complex pair: its leading real part changes from -0.100000 to 0.099570, with angular frequency 0.398506 at $r = 4$ (Fig. 3A). The homogeneous oscillation then grows faster than the stationary K mode. Its static gain remains negative, $G(6) = -7.855828$, so this change cannot be a zero-frequency crossing.

This reordering extends beyond the anchor. Among cases whose leading AS instability is stationary and K-like, the proportion led by an oscillatory mode at $r = 8$ is 62.2% across ten original-box designs and 43.1% across five wider-box designs (Fig. 3B). At $r = 32$ the corresponding proportions are 77.7% and 54.4%. The overall unstable fractions change much less: from 37.4% to 39.0% in the original box and from 28.9% to 29.7% in the wider box between $r = 1$ and 32. These two percentages use different denominators: the switching proportion is conditional on initially stationary K-led cases, whereas the unstable fraction includes every sampled point.

Close to stationary onset, the response shape matters less. Define the plant's signed logarithmic slope $\tau_p = -L'_{0,\mu}(0)/G(\mu)$. For a downstream response with finite second moment and $\tau_p + \bar{\tau} > 0$, the real branch emerging from zero satisfies

$$\sigma = \frac{G - 1}{G(\tau_p + \bar{\tau})} + O((G - 1)^2). \tag{7}$$

Thus equal gain and mean response time match growth to first order near onset, although they need not match it farther away (Fig. S1B). The plant term is a signed slope and need not itself be a positive physical delay. These results concern the linearisation at the homogeneous state; a faster oscillatory mode does not by itself establish a stable nonlinear oscillation.

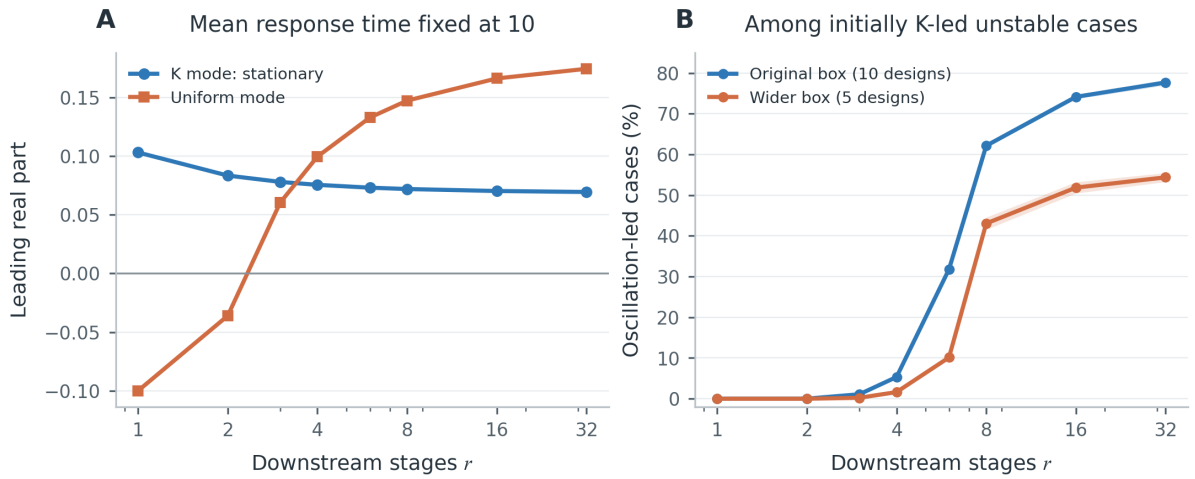


Figure 3: Pathway resolution changes mode competition without changing the mean time. (A) Leading real parts of the K and uniform modes at P2 for equal-stage pathways with mean time 10. The uniform branch is oscillatory for the plotted depths above one and overtakes K by depth four. (B) Fraction of initially stationary, K-led unstable cases whose leading instability becomes oscillatory. Points are means over independent 4,000-point designs; bands are approximate 95% Monte Carlo intervals computed across ten original-box or five wider-box designs. They describe variation under the sampling measure.

3.3 Matching linear feedback does not determine nonlinear selection

The memory-location controls provide a stricter match. At equal response time, AS and linear AE have the same full local spectrum at every shared positive equilibrium, including heterogeneous states. Nevertheless, their nonlinear routes to these states can differ.

Selection is measured in a prescribed seven-cell competent patch within a periodic 9×9 graph. Competence is one inside and 0.02 outside; the centre has an imposed production factor of 1.5 or 3. A candidate must have high proneural and low NICD-like activity while the other competent cells remain suppressed for ten time units (Methods). This measures sustained molecular contrast within an imposed field.

Proneural activity is examined directly rather than inferred from Delta contrast. In the first weak-bias P3 neighbourhood vector and its first paired start, AS retains one ASC-high cell, whereas linear AE retains three (Fig. 4A). The ASC-high cells also have elevated Delta and low activated Notch: AS selects the centre, whereas AE selects three neighbours. The cell-level fields and ASC time courses are retained with the source data. The same physical cells and colour scale are used across the two ASC maps. Independent tighter Radau integrations reproduce the complete recorded candidate and identity sequences. Here S represents aggregate ASC activity; it does not resolve separate achaete and scute expression or a downstream fate switch.

Across 24 nearby parameter vectors and two paired starts per vector, weak-bias P3 gives maintained single candidates in 38/48 AS runs and 0/48 AE runs (Fig. 4C). AS has more maintained candidates in 19 vectors, with five ties. Both models can locally maintain the same single-candidate equilibria in the tested anchor controls. The difference therefore concerns access to shared states, rather than their existence alone.

Exchanging response times within AES makes the same point without removing either stage. Let τ_0 be each vector's baseline ASC response time. The allocations $(\tau_S, \tau_E) = (\tau_0, 4\tau_0)$ and $(4\tau_0, \tau_0)$ have identical linear loops and local spectra. At weak-bias P3, however, they maintain a single candidate in 12/48 and 26/48 starts, respectively (Fig. 4D). Seven parameter vectors differ and 17 tie; the paired difference in maintained proportion is -29.2 percentage points, with a vector-bootstrap 95% interval of $[-50.0, -12.5]$. Strong bias gives 48/48 for both allocations.

The direction and size of the contrast therefore depend on the competent field and operating point.

At the P2 anchor with centre factor 1.5, exchanging $(10, 40)$ and $(40, 10)$ changes confirmation from 144.5 to 206.5 in all four paired starts. This timing order is not universal: two eligible weak-bias P2 neighbourhood vectors reverse it. The P3 loss of single selection under faster ASC turnover also disappears in tested anchor controls with larger initial perturbations or matched nonlinear E induction. These controls constrain the interpretation to the specified laws and initial fields.

A finite input tests whether these realisations can be distinguished beyond their matched local spectra. At P2, doubling clamped A separates the AS and linear-AE S responses by up to 32.6% of their common steady-state change (Fig. 4B). This distinguishes the specified response laws, but does not uniquely locate the memory. For fixed competence, let $C_i = \chi_i \lambda_S / d_S$. The saturating mediator

$$\tau_S \dot{E}_i = 1 - h_S(A_i) - E_i, \qquad S_i = C_i(1 - E_i) \tag{8}$$

gives $\tau_S \dot{S}_i = C_i h_S(A_i) - S_i$, exactly the AS equation. Mapped initial conditions therefore reproduce every AS D,N,A,S trajectory; on $0 \le S_i \le C_i$, E also lies in $[0, 1]$. Finite-input discrimination of a linear E control and identification of the biological carrier of memory are separate questions.

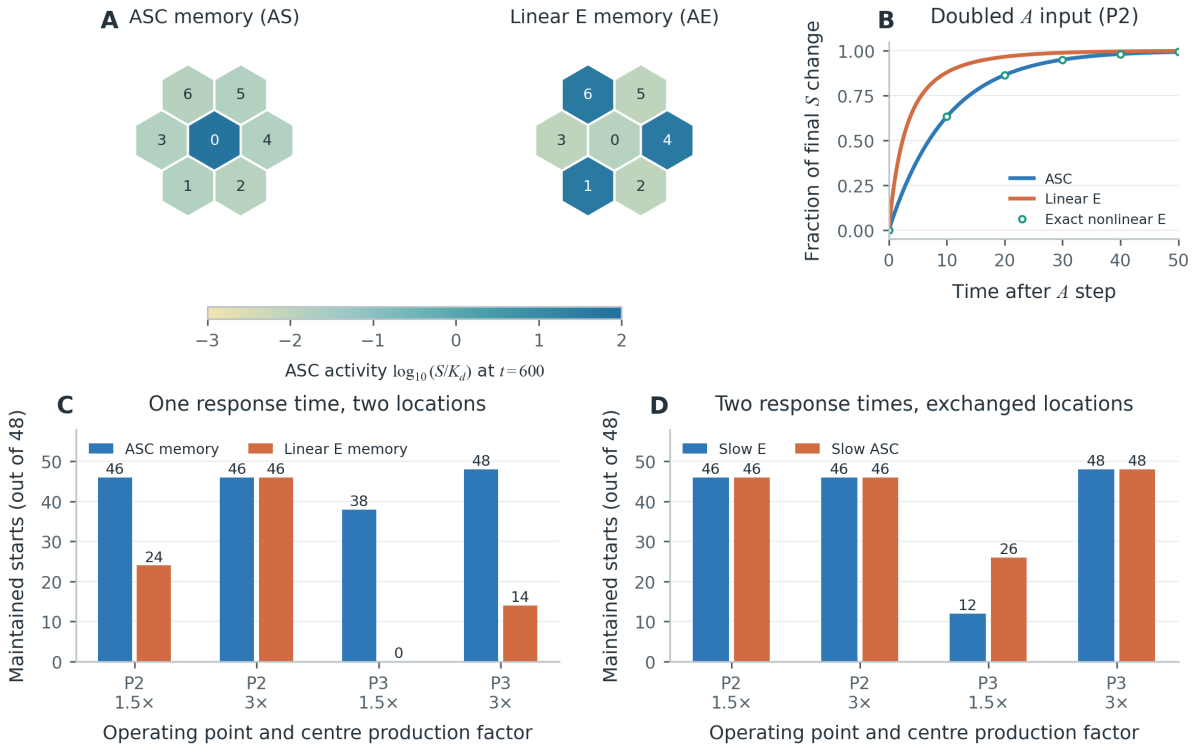


Figure 4: Matched linear feedback leaves molecular selection and finite-input responses unresolved. (A) ASC activity at time 600 in the seven competent cells, for AS (left) and linear AE (right), using the first weak-bias P3 neighbourhood vector and first seed. Both maps use the same logarithmic scale and cell numbering; 0 is the centre. Polygons depict contact topology, not measured cell shapes. (B) At P2, a doubled clamped-A input separates AS from linear AE, while the exact nonlinear E realisation overlays AS. Responses are scaled by their common final S change. (C) Maintained single-candidate counts for AS and AE at equal response time. (D) AES with exchanged slow-E/slow-ASC response times. Each bar comprises 48 starts nested within 24 paired parameter vectors; the vector is the statistical unit. Counts include prescribed extensions.

4 Discussion

The matched comparisons identify three distinct requirements for predicting Notch–Delta patterning. Static gain fixes the stationary boundary. The cis/trans condition in Eq. 6 also makes it an exact stability test within a negative-mode block, providing a concrete comparison with graph-based input–output criteria. Frequency-dependent feedback determines linear growth and the competition with oscillatory modes. Nonlinear response laws and the placement of kinetic stages can still matter after the local linear response has been matched. Agreement at one level does not establish agreement at the next.

Earlier lateral-inhibition models linked signalling delay to oscillatory dynamics [11] and defect suppression [12]. In mouse neural progenitors and presomitic mesoderm, altered Dll1 expression timing also changes oscillatory dynamics [13]. The comparison here holds the complete static response and the mean downstream time fixed, so the finite-chain mode reordering is attributable to response shape. The gain and peak-gain certificates apply standard feedback arguments; they bound admissible pathways rather than introduce a new general instability criterion.

In a long-range Notch–Delta model with cell protrusions, Berkemeier and Page found that linear and multiscale analyses explain only part of pattern selection, with additional contributions from nonlinear effects [14]. The matched-spectrum comparisons here isolate one such limitation: identical local linear responses can lead to different sustained ASC selections under the same prescribed initial fields.

The exact realisation in Eq. 8 limits molecular attribution. Distinguishing a specified linear E law from ASC relaxation does not exclude a nonlinear E law that reproduces the same outputs. Direct E measurements or independently constrained induction and repression laws are needed to identify the carrier of feedback memory.

A prospective test would change proneural production and degradation together, verify that the complete static response remains matched, and measure the time-resolved proneural, activated-Notch and Delta responses. An independently constrained repressor intervention supplies the complementary comparison. Matching only the mean response time would be insufficient if response shape changes. Reporter maturation and turnover would also need separate measurement. These are proposed tests; the present parameters are not calibrated to a tissue.

Several limits remain. The contact graph and competent patch are prescribed. Within the regular-graph formulation, the exact-gain condition at the most negative mode depends on the contact spectrum through $\mu_{\min}$. Three-dimensional epithelial contacts can increase the number of signalling neighbours and alter SOP spacing [15]; extending the present comparison to such tissue-derived graphs requires their contact structure to be specified. Parameter fractions depend on sampling bounds. The pathway-resolution results establish changes in linear mode competition, without claiming persistent nonlinear cycles or a completed nonlinear cascade survey. A finite set of local stability and solver checks does not establish global basin structure. Finally, sustained molecular selection is distinct from endogenous competence, lineage specification and irreversible commitment. Within these limits, the comparisons specify which kinetic information is missing when static feedback alone is used to predict a spatial outcome.

5 Methods

Homogeneous equilibria were found by Brent bracketing after scalar elimination of N, A, S. The 54 distinct adjacency eigenvalues of the periodic reference lattice were scanned, including the uniform mode. The stationary threshold was located independently using the leading pole and $G(-3) - 1$, with root tolerance 10^{-13}. Full eigenvalues and Nyquist counts were compared at all 4,000 reference points. The mode-positivity comparison recomputed their equilibria and

K-block spectra and exhaustively checked all eight diagonal signatures modulo a common sign. Equal-stage pathways were evaluated by direct eigenvalues of their $(3 + r)$-state mode blocks for $r = 1, 2, 3, 4, 6, 8, 16, 32$. Peak gain was evaluated at zero and the nonnegative stationary points of $|L_0(i\omega)|^2$ as a rational function of ω^2, with independent dense-frequency checks.

The reference and replicate Latin-hypercube designs use log-uniform rates and constants in $[0.1, 10]$ times their baseline values, and uniform Hill exponents in $[1, 6]$. Five wider-box designs use $[0.01, 100]$ times baseline for rates and constants. Each design has 4,000 points. Replicate-level intervals describe numerical sampling variation. Near-onset checks use the reference and ten original-box designs with positive $\tau_p + \bar{\tau}$.

In the patch, a candidate satisfies $h_D(S) \geq 0.8$ and $h_S(A) \geq 0.8$; every other competent cell must satisfy both responses ≤ 0.2 for the same ten-unit interval. The central bias remains applied. Maintained selection additionally requires no subsequent loss and a single candidate at the final observation horizon. Neighbourhood vectors vary all 13 parameters over $[0.8, 1.25]$ times each anchor, with two paired starts. Initial physical fields are matched within each comparison. Statistical comparisons resample the 24 parameter vectors, retaining the nested starts, using 20,000 fixed-seed bootstrap draws.

Nonlinear production runs use adaptive BDF integration with relative tolerance 10^{-9}, absolute tolerance 10^{-12} and maximum step 0.5, with tighter BDF and independent Radau checks at relative tolerance 10^{-11} and absolute tolerance 10^{-14} for the reported turnover controls. Confirmation is recorded at intervals of 0.5; it is not interpreted with finer timing precision. Prescribed extensions and residual criteria distinguish unconfirmed or drifting endpoints from maintained outcomes. Exact-eigenvector growth checks, numerical tolerances, independent molecular-field reintegrations and the numerical audit are given in the Supplementary Material below.

Acknowledgements

I thank Professor Philip Nelson for helpful discussions and feedback.

Data and code availability

The project repository is `https://github.com/HyeonjeYang/notch-delta-feedback-patterning-v2`. Version-specific figure data and numerical audits, including `audit_signed_mode_gain.py`, are supplied in the separate author reproducibility archive. The Overleaf package contains the manuscript sources and publication figures.

Supplementary Material

Matched static feedback permits different Notch–Delta patterning dynamics

S1 Analytic checks

On a degree-z regular graph ($z = 6$ here), the homogeneous steady state satisfies

$$N(D) = \frac{\lambda_N}{d_N + (zf_N + k_c)D}, \quad A(D) = \frac{zf_N N(D) D}{d_A}, \quad S(D) = \frac{\lambda_S}{d_S} h_S(A(D)). \tag{S1}$$

The remaining scalar equation is

$$F(D) = \lambda_D h_D(S(D)) - d_D D - (zf_D + k_c) D N(D) = 0. \tag{S2}$$

As D increases, N and S decrease and A increases. Production in F decreases, while its total loss increases strictly. Since $F(0) > 0$ and $F(\lambda_D/d_D) < 0$, the positive homogeneous equilibrium is unique. Brent bracketing uses this interval, relative tolerance $4\epsilon_{\mathrm{mach}}$ and the smallest positive normal floating-point number as absolute tolerance.

Write a_{ij} for entries of the D,N,A plant B_μ. Its D,N block has negative trace and determinant

$$\Delta(\mu) \geq d_D d_N + d_D(zf_N + k_c)D^* + d_N(zf_D + k_c)N^* > 0 \tag{S3}$$

for $|\mu| \leq z$; the remaining plant pole is $-d_A$. Thus the plant is Hurwitz. The Schur identity gives $\det J_\mu = \det B_\mu(-d_S)(1 - G)$: unity gain is the zero-pole condition, while gain below one does not exclude an unstable pair.

Set $\gamma = \lambda_D h'_D(S^*)[-\lambda_S h'_S(A^*)/d_S] f_N N^*/d_A > 0$. Then $G(\mu) = \gamma\nu(\mu)/\Delta(\mu)$, where $\nu(\mu) = zk_cD^* - \mu(d_N + k_cD^*)$ decreases linearly. It is negative at z. Between $\mu_{\min}$ and the zero of ν, the quadratic $\nu(\mu_{\min})\Delta(\mu) - \nu(\mu)\Delta(\mu_{\min})$ is concave, zero at the left endpoint and positive at the right. It is positive inside, proving that static gain is maximal at $\mu_{\min}$. For the triangular lattice, $\mu = 2\cos k_1 + 2\cos k_2 + 2\cos(k_1 - k_2)$, with $k_1 = 2\pi a/24$, $k_2 = 2\pi\ell/24$ and $a, \ell = 0, \ldots, 23$; its minimum is -3.

For a stable pathway with nonnegative unit-area impulse response, $H(0) = 1$ and $|H(i\omega)| \leq 1$. If G exceeds one, the real loop $L_0(s)H(s)$ crosses one between zero and positive infinity. If $\sup_\omega |L_0(i\omega)| < 1$, small gain excludes unstable roots. Neither certificate decides the remaining cases at a specified mean time. With finite second moment, $L_0H = G[1 - (\tau_p + \bar{\tau})s + O(s^2)]$ gives the main-text first-moment law when $\tau_p + \bar{\tau} > 0$. It describes the real branch emerging from zero, not necessarily the dominant complex root.

For $\mu < 0$, the fixed signs $J_{AN} > 0$, $J_{AD} < 0$, $J_{DS} > 0$ and $J_{SA} < 0$ force the diagonal signature $Q = \mathrm{diag}(1, -1, -1, 1)$, up to a common sign. The two remaining conditions for $QJ_\mu Q$ to be Metzler (nonnegative off-diagonal entries) are $J_{DN} \leq 0$ and $J_{ND} \leq 0$. Since these entries are $-D^*(k_c + \mu f_D)$ and $-N^*(k_c + \mu f_N)$, this is equivalent to $k_c \geq -\mu \max(f_D, f_N)$. The transformed plant is Hurwitz Metzler and the transformed feedback vectors are nonnegative. The scalar positive-feedback stability condition is therefore exactly $G(\mu) < 1$; at unity gain there is a zero pole, and above unity there is a positive real pole. This establishes linear mode-block positivity, without establishing monotonicity of the nonlinear cell input–output system.

S2 Essential numerical controls

The reference Latin hypercube uses seed 20260817. Original-box replicates use 2026101701–2026101710 and wider-box replicates 2026101801–2026101805, retaining parameter order and SciPy's legacy `seed=` convention. Bounds and readouts are defined in main-text Methods. The statistical unit is the parameter vector, with paired starts kept together.

Growth starts at $x^* + \varepsilon v \cos\phi$, using one scalar for the entire biochemical eigenvector. The fitting window ends when the Delta K-mode amplitude reaches $10^{-3}D^*$. P2 predicted/fitted rates are 0.1030667/0.1030769 on $[0, 67.25]$; P3 gives 0.216300/0.216305 on $[0, 32]$ (Fig. S1A). The first-moment error decreases towards onset (Fig. S1B).

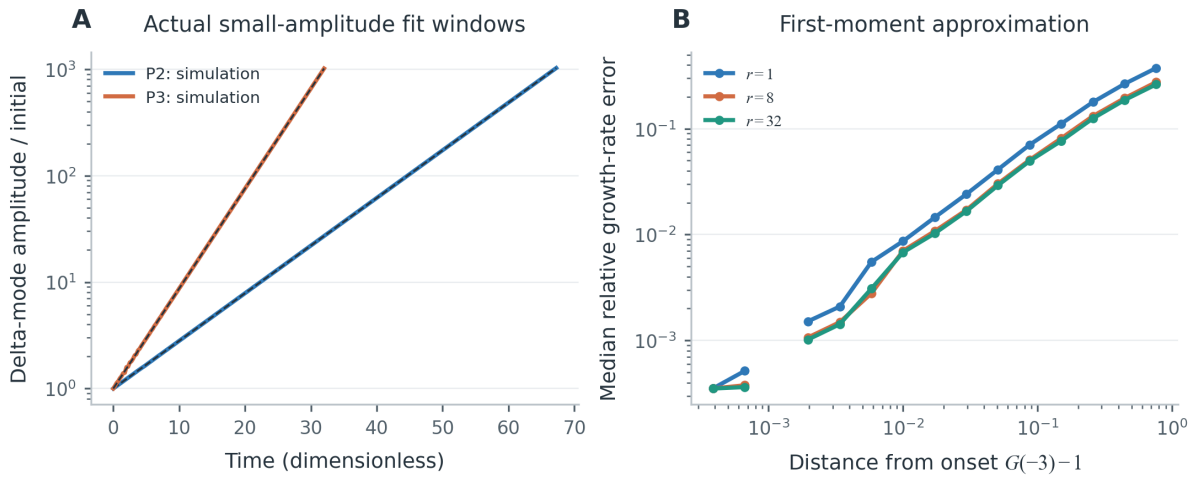


Figure S1: Growth checks. (A) Simulated amplitudes in the actual fitting windows; dashed lines are linear predictions with the same starting amplitude. (B) Binned median relative error of the first-moment approximation against exact K-mode rates, using the reference and original-box designs with positive total slope.

All eight diagonal signatures, modulo a common sign, were checked at each reference point. The sign criterion and direct signature search agreed at all 4,000 points. Of the twelve gain disagreements, five were among the 733 equilibria missed by the original solver; restoring them increases the count from seven to twelve.

The independent 4,000-point audit gives maximum normalised equilibrium residual 2.76×10^{-15} and zero K-mode Nyquist/eigenvalue count disagreements. Recalculation of 1,296 finite-chain operating-point rows differs by at most 2.67×10^{-14}. At 256 fixed parameter vectors and depths 1, 4, 8 and 32, retained-mode pole differences stay below 6.60×10^{-13}. Modes with peak gain strictly below one may be omitted from stored sample searches because their stability is certified; negative stored maxima then describe retained modes, not the full slowest decay rate.

The molecular example is P3_00, seed 2026102401, selected by order rather than effect size. AE's fourth state is E, so ASC is reconstructed as $q_i(E_i)$; it agrees with the deposited S records. Independent tight Radau runs to 600 reproduce all recorded candidate counts and identities, with maximum D,N,A,S errors scaled by $\max(1, |x|)$ of 5.44×10^{-8} (AS) and 2.32×10^{-7} (AE). Threshold/dwell controls span high thresholds $0.7, 0.8, 0.9$ and durations $5, 10, 20$. Compatible linear initialisation and complete-network endpoint spectra are retained with the source controls.

Seventy independent adaptive comparisons change emergence times by at most 0.01631%. Coarse fixed RK4 steps 0.04/0.08 fail at the stable reference point in Table 1 of the main text and were not production settings. Complete audit tables, seeds and unused extended plots remain in the author records. The incomplete nonlinear cascade survey is excluded; no persistent-cycle or irreversible-fate conclusion is drawn.

References

[1] J. R. Collier, N. A. M. Monk, P. K. Maini, J. H. Lewis. Pattern formation by lateral inhibition with feedback: a mathematical model of Delta–Notch intercellular signalling. *J. Theor. Biol.* 183, 429–446 (1996). doi:10.1006/jtbi.1996.0233

[2] D. Sprinzak, A. Lakhanpal, L. LeBon, L. A. Santat, M. E. Fontes, G. A. Anderson, J. Garcia-Ojalvo, M. B. Elowitz. Cis-interactions between Notch and Delta generate mutually exclusive signalling states. *Nature* 465, 86–90 (2010). doi:10.1038/nature08959

[3] D. Sprinzak, A. Lakhanpal, L. LeBon, J. Garcia-Ojalvo, M. B. Elowitz. Mutual inactivation of Notch receptors and ligands facilitates developmental patterning. *PLoS Comput. Biol.* 7, e1002069 (2011). doi:10.1371/journal.pcbi.1002069

[4] E. Teomy, D. A. Kessler, H. Levine. Ordered hexagonal patterns via Notch–Delta signaling. *Phys. Biol.* 18, 066006 (2021). doi:10.1088/1478-3975/ac28a4

[5] B. Jennings, J. de Celis, C. Delidakis, A. Preiss, S. Bray. Role of Notch and achaete-scute complex in the expression of Enhancer of split bHLH proteins. *Development* 121, 3745–3752 (1995). doi:10.1242/dev.121.11.3745

[6] C. V. Cabrera. Lateral inhibition and cell fate during neurogenesis in *Drosophila*: the interactions between *scute*, *Notch* and *Delta*. *Development* 110 (1), 733–742 (1990). Corrected republication with original pagination. PMID:1709404

[7] J. Culí, J. Modolell. Proneural gene self-stimulation in neural precursors: an essential mechanism for sense organ development that is regulated by Notch signaling. *Genes Dev.* 12, 2036–2047 (1998). doi:10.1101/gad.12.13.2036

[8] H. J. Wearing, M. R. Owen, J. A. Sherratt. Mathematical modelling of juxtacrine patterning. *Bull. Math. Biol.* 62, 293–320 (2000). doi:10.1006/bulm.1999.0152

[9] M. Arcak. Pattern formation by lateral inhibition in large-scale networks of cells. *IEEE Trans. Autom. Control* 58, 1250–1262 (2013). doi:10.1109/TAC.2012.2231571

[10] K. J. Åström, R. M. Murray. *Feedback Systems: An Introduction for Scientists and Engineers*, 2nd ed. Princeton University Press (2021). Author-maintained companion site

[11] H. Momiji, N. A. M. Monk. Oscillatory Notch-pathway activity in a delay model of neuronal differentiation. *Phys. Rev. E* 80, 021930 (2009). doi:10.1103/PhysRevE.80.021930

[12] D. S. Glass, X. Jin, I. H. Riedel-Kruse. Signaling delays preclude defects in lateral inhibition patterning. *Phys. Rev. Lett.* 116, 128102 (2016). doi:10.1103/PhysRevLett.116.128102

[13] H. Shimojo, A. Isomura, T. Ohtsuka, H. Kori, H. Miyachi, R. Kageyama. Oscillatory control of Delta-like1 in cell interactions regulates dynamic gene expression and tissue morphogenesis. *Genes Dev.* 30, 102–116 (2016). doi:10.1101/gad.270785.115

[14] F. Berkemeier, K. M. Page. Coupling dynamics of 2D Notch–Delta signalling. *Math. Biosci.* 360, 109012 (2023). doi:10.1016/j.mbs.2023.109012

[15] G. Paci, F. Berkemeier, B. Baum, K. M. Page, Y. Mao. 3D epithelial cell topology tunes signaling range to promote precise patterning. *Proc. Natl. Acad. Sci. USA* 123(19), e2522727123 (2026). doi:10.1073/pnas.2522727123

Figures

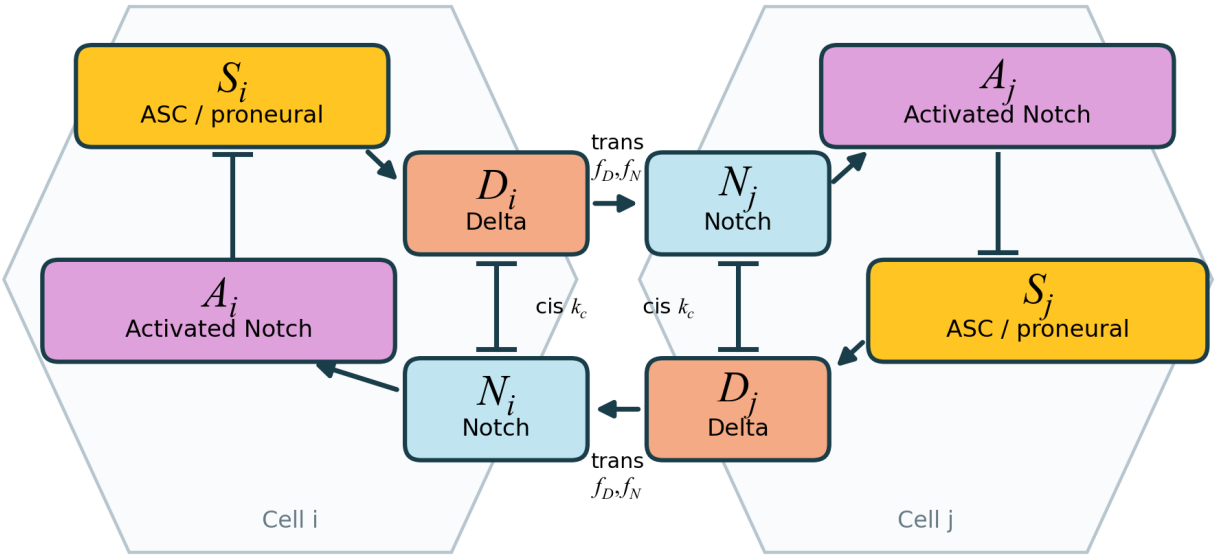


Figure 1

{The Notch--Delta--ASC feedback circuit.} Two contacting cells are shown in the layout of the supplied schematic. ASC promotes Delta; neighbour Delta activates Notch signalling, and activated Notch represses ASC. Blunt terminals indicate repression or mutual cis inactivation (k_c). Trans interactions include ligand and receptor depletion (f_D,f_N); their arrows indicate signalling, not production of receptor

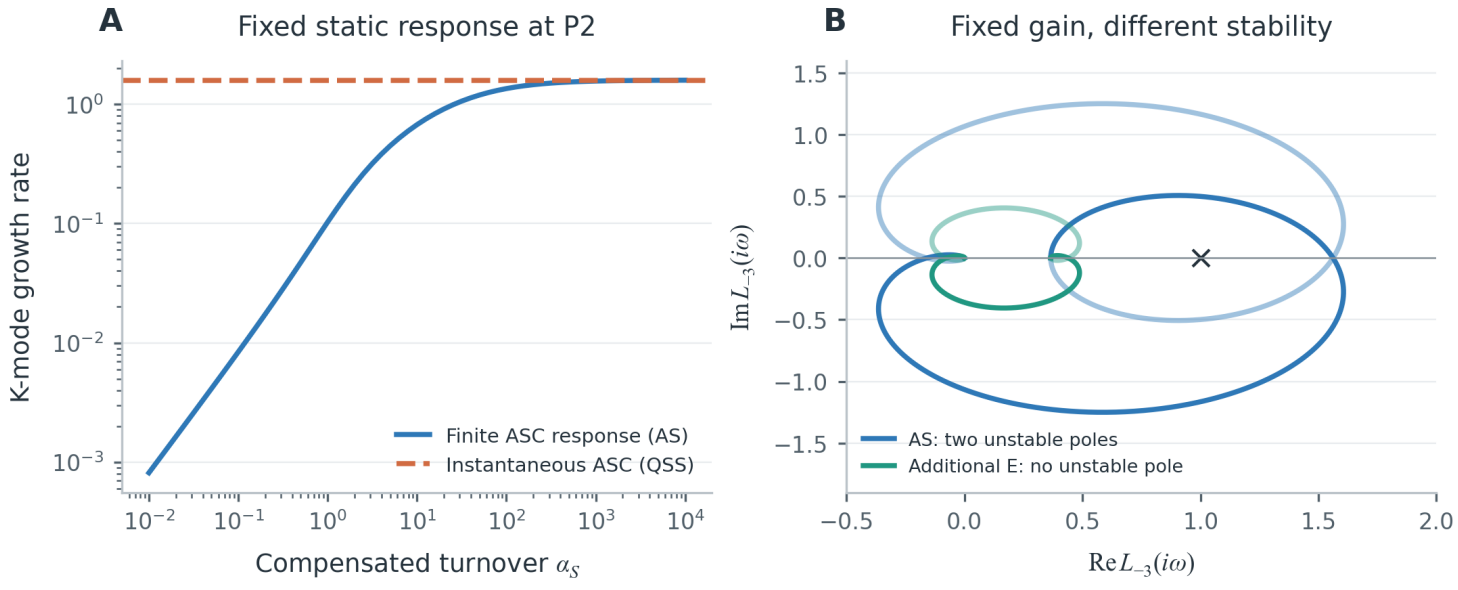


Figure 2

{Equal static feedback permits different dynamics.} (A) Compensated ASC turnover at P2 changes the K-mode growth rate while preserving the static response and stationary threshold. The dashed line is the matched quasi-static ASC reduction (QSS). (B) K-mode Nyquist curves for reference sample 1730, before and after adding E relaxation with response time 10. Both have DC gain 0.365644; the numbers of unstable poles are two and zero, respectively. The cross marks $+1$, and lighter lines show conjugate branches. All times and rates use dimensionless model units.}

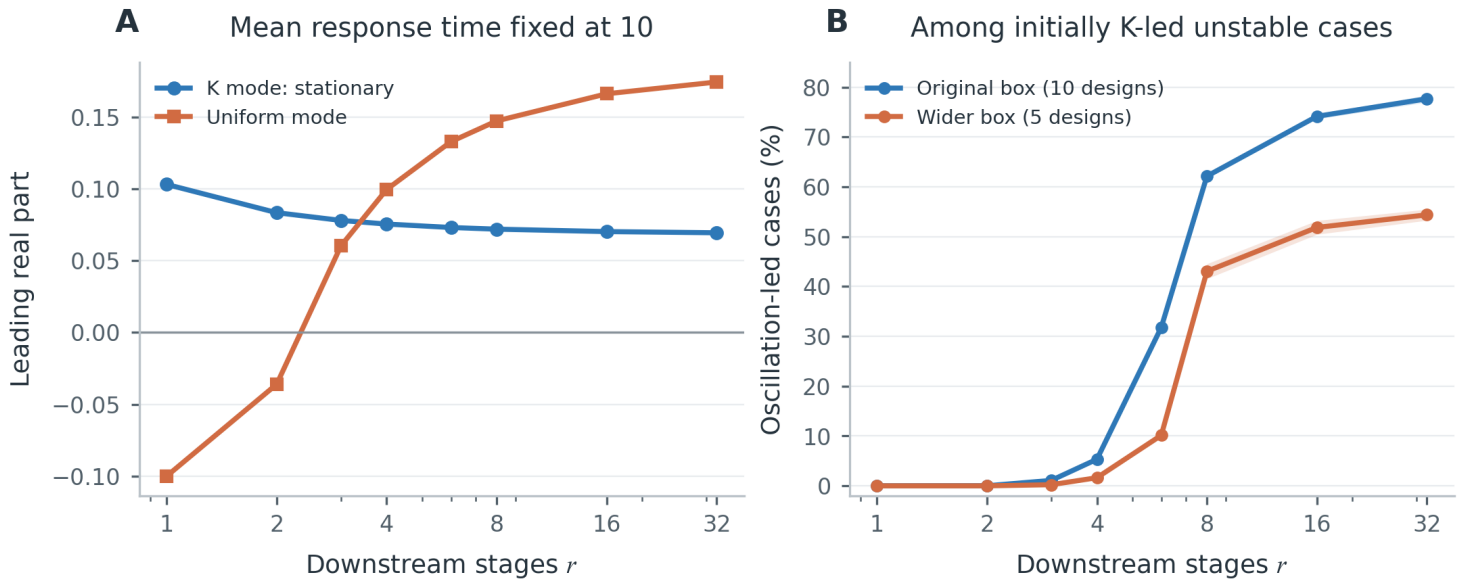


Figure 3

{Pathway resolution changes mode competition without changing the mean time.} (A) Leading real parts of the K and uniform modes at P2 for equal-stage pathways with mean time 10. The uniform branch is oscillatory for the plotted depths above one and overtakes K by depth four. (B) Fraction of initially stationary, K-led unstable cases whose leading instability becomes oscillatory. Points are means over independent 4,000-point designs; bands are approximate 95\% Monte Carlo intervals computed across ten original-box or five wider-box designs. They describe variation under the sampling measure.}

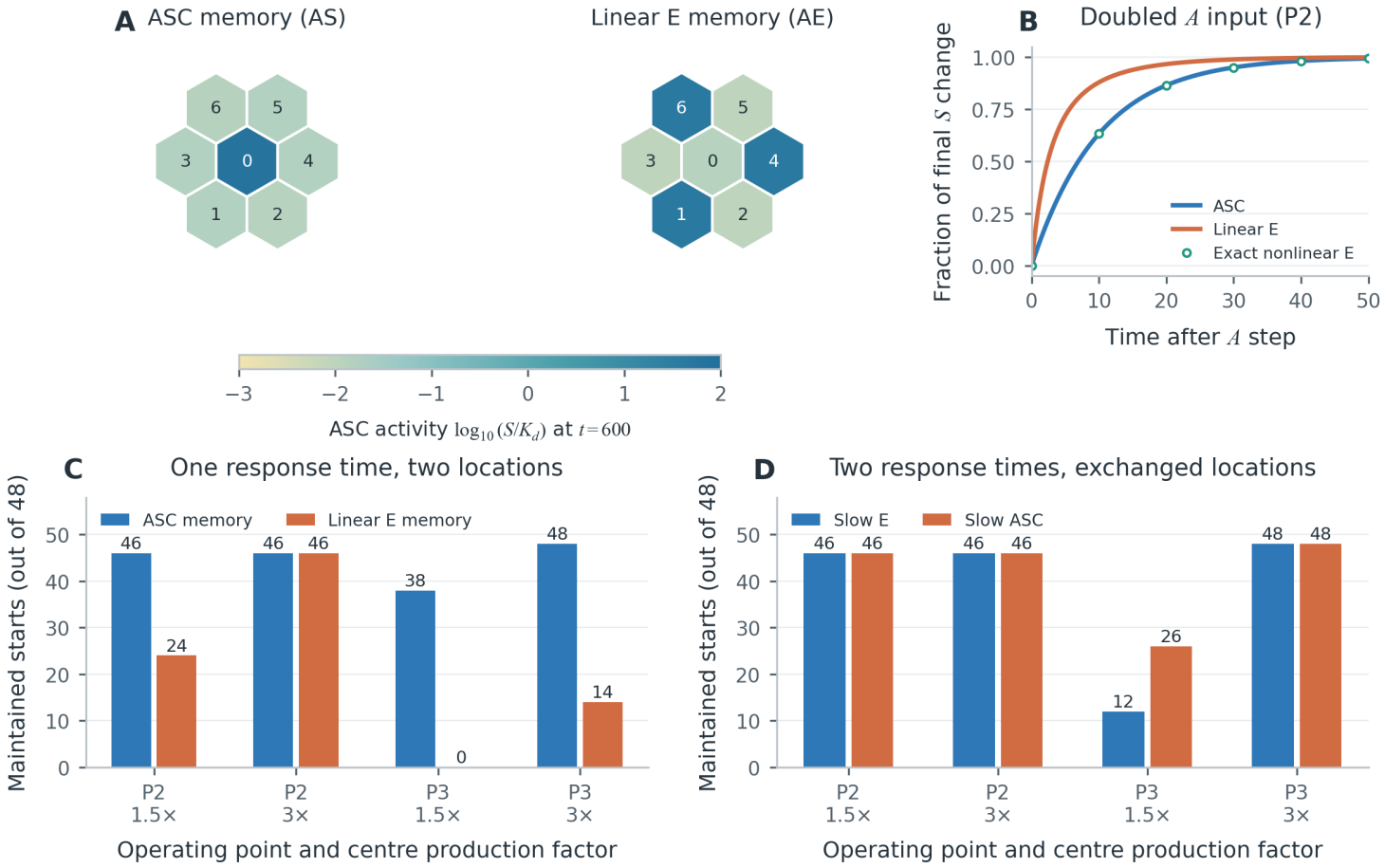


Figure 4

{Matched linear feedback leaves molecular selection and finite-input responses unresolved.} (A) ASC activity at time 600 in the seven competent cells, for AS (left) and linear AE (right), using the first weak-bias P3 neighbourhood vector and first seed. Both maps use the same logarithmic scale and cell numbering; 0 is the centre. Polygons depict contact topology, not measured cell shapes. (B) At P2, a doubled clamped-A input separates AS from linear AE, while the exact nonlinear E realisation overlays AS. Responses are scaled by their common final S change. (C) Maintained single-candidate counts for AS and AE at equal response time. (D) AES with exchanged slow-E/slow-ASC response times. Each bar comprises 48 starts nested within 24 paired parameter vectors; the vector is the statistical unit. Counts include prescribed extensions.}

Supplementary Files

This is a list of supplementary files associated with this preprint. Click to download.

- FigS1growthcontrols.png